ORIGINAL ARTICLE

Open Access

Pulsed Unipolar-Polarisation Plasma Electrolytic Polishing of Ni-Based Superalloys: A Proof of Conception

Chuanqiang Zhou[1,2], Ning Qian[1,2*] , Honghua Su[1*], Jingyuan He[1], Wenfeng Ding[1] and Jiuhua Xu[1]

Abstract

The enhanced performance of aerospace equipment drives parts development towards integration, complexity, and structural optimization. This advancement promotes metal near-net fabrication technologies like wire electrical discharge machining (WEDM) and 3D printing. However, the high initial surface roughness from WEDM or 3D printing poses significant challenges for the high-performance surface finishing required. To effectively reduce the surface roughness of the workpieces with high initial surface roughness, this paper proposes pulsed unipolar-polarisation plasma electrolytic polishing (PUP-PEP). The study examined the material removal mechanisms and surface polishing quality of PUP-PEP. This technique combines the high current density and material removal rate of the electrolytic polishing mode with the superior surface polishing quality of PEP through voltage waveform modulation. For an Inconel-718 superalloy part fabricated by WEDM, PUP-PEP reduced surface roughness from R_a 7.39 μm to R_a 0.27 μm in 6 min under optimal conditions. The roughness decreased from R_a 7.39 μm to R_a 0.78 μm in the first 3 min under pulsed unipolar-polarisation voltage, resulting in a remarkable 233% increase in efficiency compared to that with conventional PEP. Subsequently, the voltage output voltage is transformed into a constant voltage mode, and PEP is continued based on PUP-PEP to finally reduce the workpiece surface roughness value to R_a 0.27 μm. The proposed PUP-PEP technology marks the implementation of 'polishing' instead of conventional rough-finish machining processes, presenting a new approach to the surface post-processing of metal near-net fabrication technologies.

Keywords Pulsed unipolar-polarisation, Plasma electrolytic polishing, Voltage waveform, Superalloy, Surface roughness, Material removal rate

1 Introduction

The rapid advancement of metal net-shaping technologies, such as three-dimensional (3D) printing and wire electrical discharge machining (WEDM), is transforming key components in advanced manufacturing sectors, such as aerospace, making them increasingly lightweight and complex as they move toward integrated structural functionality [1]. Within specialised operational environments, these components place stringent demands on surface quality. Achieving precise surface effects often involves multiple processes, including rough machining (e.g., turning, milling, and grinding) as well as intricate semi-finishing and finishing procedures. However, parts manufactured using metal net shaping techniques often exhibit intricate structures and high surface roughness, presenting substantial challenges for subsequent processing [2, 3]. This has emerged as a technological bottleneck constraining the further advancement and application of metal net-shaping technologies [4, 5]. Furthermore, to

*Correspondence:
Ning Qian
n.qian@nuaa.edu.cn
Honghua Su
shh@nuaa.edu.cn
[1] Jiangsu Key Laboratory of Precision and Micro-Manufacturing Technology, Nanjing University of Aeronautics and Astronautics, Nanjing 210016, China
[2] JITRI Institute of Precision Manufacturing, Nanjing 211806, China

Zhou *et al. Chinese Journal of Mechanical Engineering*   (2024) 37:105

Page 2 of 17

maintain the dimensional accuracy of the external form of the component, sufficient machining allowance must be retained during the forming and manufacturing processes. Nevertheless, this requirement results in a partial loss of the inherent advantages of net-shaping manufacturing technology. Thus, it is essential to develop a novel technology that can directly machine 3D printed or WEDM parts with high surface roughness to narrow the aforementioned gap [6].

Plasma electrolytic polishing (PEP) is a rapidly developing non-valve metal surface polishing process that can remarkably improve the surface quality of the workpiece within a short time frame of 3 to 10 min [7–9]. PEP has garnered significant attention as an emerging, efficient, and environmentally friendly metal surface-polishing technology. During this process, a low-concentration salt solution serves as the electrolyte, and the workpiece is enclosed in a vapour gaseous envelope (VGE) due to the Joule heating effect, leading to luminescence and exothermic reactions [10, 11]. Traditional PEP requires immersion of the workpiece in an electrolyte and the application of a constant DC voltage ranging from 250 to 400 V. This process enables the polishing and deburring of complex workpiece surfaces [12, 13].

Although traditional PEP has unique advantages in reducing the surface roughness of complex workpieces, it has significant limitations that cannot be ignored. Fully immersing the workpiece in the electrolyte does not allow selective processing of the workpiece surface. Prolonged processing, due to the sharp-point effect of the electric field distribution, can compromise the dimensional accuracy of the workpiece, particularly affecting sharp corners and edges [14, 15]. Additionally, the size of the electrolytic cell and power supply restrict the dimensions of the workpieces that can be processed. To address these issues, researchers have proposed the spray PEP method as an alternative to the traditional immersion-based approach [16–18]. Furthermore, the final surface roughness of the processed workpiece is significantly influenced by the initial surface roughness [9, 19]. During the PEP process, the state and properties of the VGE significantly impact polishing and efficiency [20]. The VGE, primarily composed of water vapor, is crucial for realising PEP. Compared with the electrolyte (0.65 S/m), the conductivity of the VGE is much smaller (2.55×10^{-4} S/m), resulting in much lower current densities for PEP [12]. In the PEP process, the current density ranges from 0.3 to 0.7 A/cm^2, which is considerably less than the 10 to 50 A/cm^2 required for electrolysis [21]. The normal dissolution rate of the workpiece surface during PEP is only 1 to 8 μm/min, leading to the problem of low efficiency in treating surfaces with high surface roughness [22].

The effectiveness and rate of traditional PEP depend not only on polishing parameters but also on the initial roughness of the workpiece [23]. Table 1 lists the final surface roughness values achieved by PEP for various materials. Traditional PEP is well-suited for polishing the surfaces of workpieces with a roughness of less than 3 μm [24]. Rapidly reducing the surface roughness values of workpieces under direct current stabilization while enhancing the efficiency of PEP polishing remains a challenging task, especially concerning workpiece surfaces with high roughness values such as those produced by wire electrical discharge machining and 3D printing.

To enhance the efficiency of PEP and significantly reduce the surface roughness of the workpiece, this study proposes a pulsed unipolar-polarisation plasma electrolytic polishing (PUP-PEP) process for nickel-based superalloys. Since material removal in PUP-PEP primarily hinges on electrochemical reactions, the equivalent circuit of the reaction interface layer of nickel-based superalloys was initially derived through EIS to elucidate the electrochemical behavior throughout the reaction process. Following this, under equivalent current density, a comparative analysis was undertaken regarding the surface roughness and material removal rate of workpieces in low-voltage (8 V) electrolytic mode and high-voltage (300 V) PEP mode. The effects of electrolytic mode and PEP mode on PUP-PEP were discussed. Then the process parameters of PUP-PEP were optimized by grey correlation analysis method and verified by experiment.

Table 1 Surface roughness of typical materials before and after PEP

Material	Initial surface roughness (μm)	Final surface roughness (μm)	Time (min)	Voltage range (V)	Literature reference
20X13	R_a 0.45	R_a 0.06	15	250–300	Parfenov et al. [14]
AISI 316	S_a 3	S_a 0.6	10	350	Yang et al. [25]
CoCr	R_a 3	R_a 0.015	8	450	Seo et al. [26]
Aluminum	R_a 1.2	R_a 0.2	5	280–320	Zakharov et al. [27]
Copper	0.16	0.08	1	400–550	Valiev et al. [28]
Ti-6Al-4V	R_a 0.2	R_a 0.05	10	260–280	Smyslova et al. [29]

2 Design and Conception of PUP-PEP

PUP-PEP is a kind of polishing mode that is evolved by changing voltage waveform based on traditional DC voltage regulator PEP. The range of voltage variation occurs only on the positive half axis, ensuring that the workpiece is always an anode. Electrolytic mode and PEP mode are included in this process.

PEP typically occurs within specific voltage ranges, this is because the material removal and the generation and state of the VGE are closely interrelated during the process. The formation and maintenance of the VGE require a particular input voltage. The workpiece experienced a progressive voltage escalation within the electrolyte, during which voltage and current signals were monitored to generate a dynamic current-resistance curve, depicted in Figure 1. This evolving trend can be segmented into four distinct regions [30–32]. Region (a) corresponds to the classical electrochemical reaction zone, which adheres to Faraday's first law. Region (b) signifies the range with a negative differential resistance characteristic [14], whereas Region (c) corresponds to the PEP zone. Typically, PEP occurs within the specific voltage range of 250 to 400 V [12]. When the voltage exceeds 400 V, it enters Region (d), known as the arc discharge phase. In this phase, the polishing effect diminishes, and it is accompanied by intense glow, heat, and popping noise [7].

Material removal in PEP is primarily driven by electrochemical reactions, and the material removal rate is positively correlated with the average current density on the workpiece surface [33]. Although the voltage was maintained at a relatively high value throughout the processing, the presence of the VGE, a high-resistance material, maintained the average current density in a low range. Under the traditional direct current constant voltage
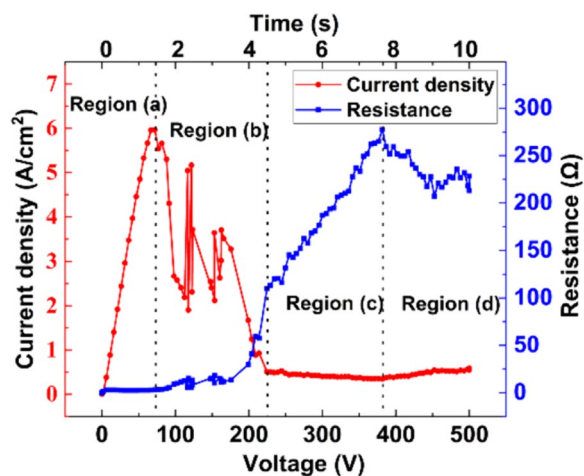
condition, the average current density during the processing remains stable at a low level of 0.35–0.5 A/cm^2, as shown in Figure 1. Consequently, the processing of large workpieces with high surface roughness requires a significant amount of time.

In the electrolysis mode, Region (a) in Figure 1 exhibits a significantly higher average current density (0.5–5.96 A/cm^2) compared to the PEP mode, as there is no presence of a VGE. Enhancing the average current density through electric field regulation is a relatively straightforward approach for improving the material removal rate during PEP. As shown in Figure 2(d), changing from direct-current (DC) voltage regulation to pulses in the unipolar-polarisation voltage led to a substantial increase in the average current density during the process, which theoretically corresponds to an increased material removal rate. This is the basic principle of PUP-PEP. In this process, the machining process undergoes electrolysis with a higher current density, followed by PEP with VGE. As depicted in Figure 2(a), in the electrolysis mode, electrochemical reactions occur between the electrolyte and workpiece surface in direct contact. In the PEP mode, the VGE consisted of numerous vapour bubbles, as illustrated in Figure 2(b). The generation and collapse of the VGE in the electrolyte forcefully impacted the workpiece surface, leading to the removal of surface products. Additionally, the strong electric field generated within the VGE triggered intense oxidation reactions, further enhancing the electrochemical reactions in the electrolysis mode. The occurrence of the discharge breakdown phenomenon was not excluded within the VGE. The impact of plasma discharge will also promote the separation of electrolytic products on the surface of the workpiece. As shown in Figure 2(c), when the voltage returns to the electrolysis mode, the electrolyte contacts the workpiece surface again, initiating electrochemical reactions and completing one cycle. In this case, the PUP-PEP can greatly improve the average current density in the polishing process, and further improve the polishing efficiency.

3 Materials and Methods

3.1 Material and the Properties of the Specimens

Ni-based superalloys find widespread use in critical aerospace components such as turbine disks and turbine casings due to their high yield strength, elevated-temperature strength, and exceptional fatigue resistance [34, 35]. Ensuring a precise surface finish on a superalloy is essential to prevent fatigue damage and prolong its overall lifespan. The workpiece is made of Inconel 718, a typical nickel-based superalloy, whose chemical elements are listed in Table 2.

Figure 1 Dynamic current density and resistance signals in different regions
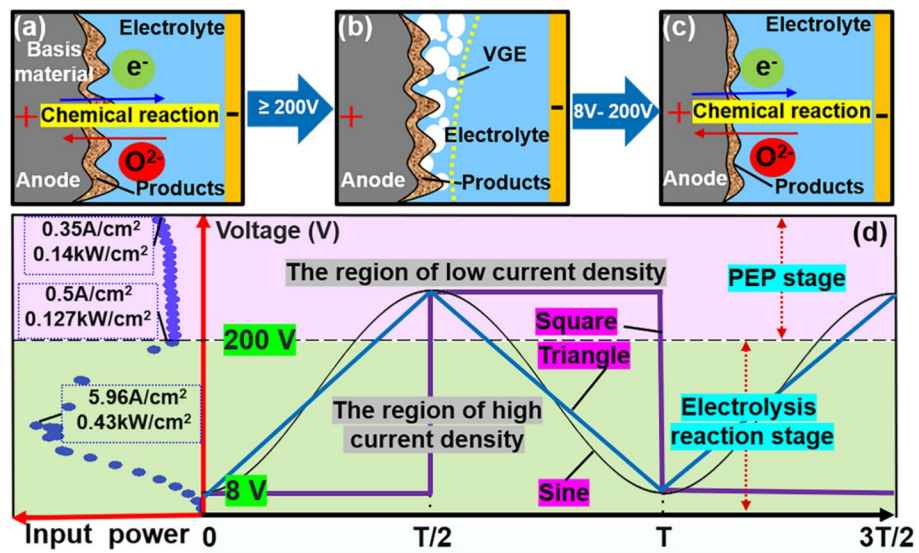
Figure 2 Design and conception of PUP-PEP: **a** Electrolytic reactions below 200 V, **b** VGE and plasma discharge removes electrolytic products, **c** Return to electrolysis mode, and **d** Variation of current density with different voltage waveforms within one cycle

**Table 2** Chemical composition of Inconel 718 superalloy [36]

Element	Composite (wt %)	Element	Composite (wt %)
Ni	52.9	C	0.03
Fe	19.2	Si	0.03
Cr	18.1	Cu	0.02
Nb + Ta	5.09	Mn	0.02
Mo	3.04	B	0.004
Ti	1.00	S	0.002
Al	0.61	P	< 0.001
Co	0.06	T.O.E	< 0.5

To maintain consistent workpiece dimensions and surface roughness, the material was cut into sample pieces measuring 10 mm×10 mm×5 mm using a WEDM machine. As depicted in Figure 3, the workpiece surface exhibits significant roughness, with a R_a value ranging from 6 to 8 μm.

3.2 Experimental Setups
A part-handling system was employed to execute linear movements in the Z-direction, ensuring proper immersion depth of the workpiece. Furthermore, the polishing system includes an electrolyte-control unit to maintain stable electrolyte parameters, including temperature and concentration [17]. Figure 4 illustrates the utilization of an ITECH programmable DC power supply (IT6000D) during the polishing process. It boasts a maximum output voltage of 1500 V and a maximum output current of 30 A, as well as the ability to capture real-time measurements of output voltage, current, and power signals.
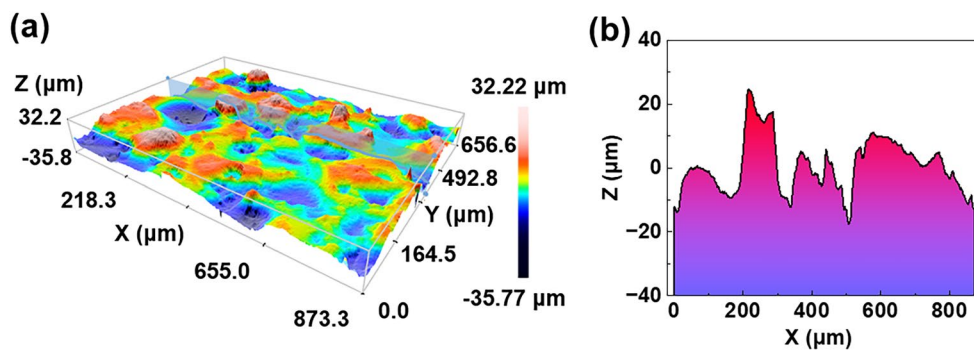
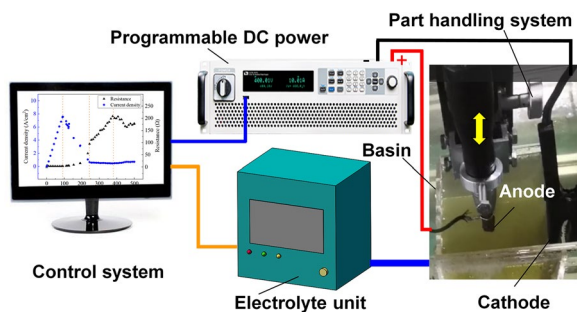**Figure 3** Surface topography of the workpiece after WEDM: **a** 3D topographic, **b** section profile

Figure 4 Schematic of the experimental devices

Table 3 Levels of factors in orthogonal experiments

Levels	A Peak voltage (V)	B Voltage waveform	C Periods (s)	D Loading time (min)
1	250	Square	0.5	1
2	300	Sine	2	2
3	350	Triangle	8	3

3.3 Design of Experiments

Initially, polarisation curve analysis of the workpiece was carried out using a multi-channel electrochemical workstation of model VSP. The scanning range is −0.1 V–5 V, and the scanning speed is 5 mV/s. The electrolyte temperature is 75 °C ± 1 °C. The critical voltage of the workpiece for electrochemical reaction is obtained. The electrochemical impedance analysis was carried out under the critical voltage, and the equivalent circuit was obtained by analyzing and fitting the data with Zview software. The contact area of the reaction surface was 1 cm^2, while insulation treatment was applied to the remaining five surfaces. The initial voltage was set at the open circuit potential, with an amplitude of 5 mV, a frequency range of 0.1 Hz–10^5 kHz, an electrolyte concentration of 3 wt%, and a temperature of 75 °C ± 1 °C.

Subsequently, a comparative analysis was conducted to assess the processing characteristics of the electrolytic and PEP modes at the same current density. The analysis focused on evaluating the current signal, surface element composition, surface morphology, and material removal rates in both modes. To ensure the accuracy of the experimental results, it was crucial to maintain consistent parameters except for the voltage. The electrolytic mode operated at a voltage of 8 V, whereas the PEP mode operated at a voltage of 300 V. Both modes utilised an electrolyte concentration of 3 wt% and a temperature of 75 °C ± 1 °C, with a processing duration of 10 min. Data were collected at 1-min intervals.

The introduction of variations in the voltage waveform brought about new factors. To minimise the number of experiments a Taguchi orthogonal design of experiments was employed. Within a specific parameter range, the grey correlation analysis method was utilised to optimise the combination of process parameters and validate them through experimentation. The orthogonal experiment involved specific process parameters,

as outlined in Table 3, incorporating four factors: peak voltage, voltage waveform, period, and loading time, with each factor having three levels. The voltage values were set within the range of PEP voltages, and the voltage waveforms were selected from three typical waveforms that span the electrolytic voltage range: sine, square, and triangular. Taking into consideration the time required for the generation of the VGE, the minimum period value was set at 0.5 s, with the other two levels being incremented by four times. It is important to note that even though non-numerical factors were included in the factors, the evaluation indicators (surface roughness, material removal rate, and current efficiency) are numerical, which will not affect the analysis results.

3.4 Surface Characterization

The workpieces underwent cleaning with alcohol using an ultrasonic cleaning machine both before and after the processing. Surface morphologies of the workpieces were assessed through scanning electron microscopy (SEM), three-dimensional video microscopy, and confocal white-light interferometry. The surface roughness of the workpiece was measured using a handheld Mahr roughness gauge (model number PS10). Three measurements were taken at distinct positions on the workpiece surface and then averaged. The weight loss of the processed workpiece was determined using a precision electronic balance with an accuracy of 0.1 mg. Three measurements were recorded and then averaged. The elemental composition of the workpiece surface was analysed using energy-dispersive spectroscopy (EDS).

The surface quality of the processed workpieces was assessed using surface roughness as the evaluation parameter, whereas the material removal rate was determined based on the normal removal quantity per unit time and current efficiency, as specified by Eq. (1). Additionally, current efficiency served as an evaluation criterion and was calculated using Eq. (2).

$$r = \frac{\Delta m}{\rho s t} \times 10^4, \tag{1}$$

Zhou *et al. Chinese Journal of Mechanical Engineering*   (2024) 37:105

Page 6 of 17

where r represents the material removal rate (μm/min), Δm is the workpiece weight loss (g), ρ denotes the material density (g/cm^3), s represents the workpiece surface area (cm^2), and t denotes the processing time (min).

$$\eta = 60 \times \frac{\Delta m}{kit} \times 100\%, \tag{2}$$

where η represents the current efficiency, Δm is the workpiece weight loss (g), k denotes the electrochemical equivalent (g/(A·h)), i is the average current during processing (A), and t denotes the processing time (min).

4 Results and Discussion

4.1 Impedance Spectroscopy Analysis

Figure 5 depicts the polarisation curve of the Inconel 718 superalloy in a 75 ℃±1 ℃ electrolyte. The self-corrosion potential of the nickel-based superalloy in the electrolyte is 41.9 mV (open-circuit voltage of 0.195 mV±0.03 mV). The critical potential at which a significant change in current density occurs is 1.32 V. When the voltage exceeds 1.32 V, the Tafel polarisation curve enters a gentle stage, and at this point, a passivation film (electrolytic product) forms on the surface of the workpiece. Failure to promptly remove the passivation film from the workpiece surface in the electrolytic mode will impede the progress of electrochemical reactions.

To gain a deeper understanding of the electrochemical behavior of the Inconel 718 superalloy in the electrolyte, Electrochemical Impedance Spectroscopy (EIS) tests were conducted at the critical voltage (1.32 V), and the test results are depicted in Figure 6(a) and (b). The final equivalent circuit diagram for the electrochemical reaction interface layer was obtained, as shown in Figure 6(c). At the reaction interface, a double-layer capacitance C is present, with an electrolyte resistance R, and R_2 represents the charge transfer resistance. Additionally, there is ion diffusion (R_1 and L). Specific values for the equivalent components are provided in Table 4.

During the process of PEP, there are charge transfer and material transfer near the surface of the workpiece. This primarily involves the electrochemical oxidation of electrons from the metal surface of the workpiece and the process of metal ions entering the electrolyte. Possible electrochemical reaction processes includes reactions in Eqs. (3)–(7).
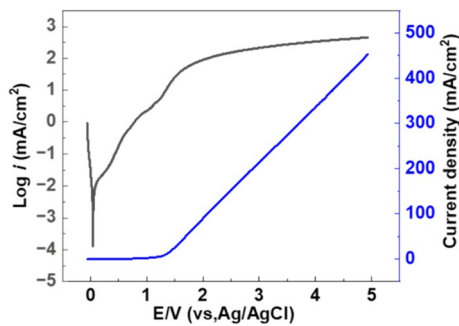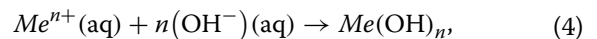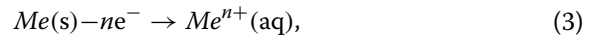
$$Me(s) - ne^- \rightarrow Me^{n+}(aq), \tag{3}$$

$$Me^{n+}(aq) + n(OH^-)(aq) \rightarrow Me(OH)_n, \tag{4}$$

Figure 5 Polarisation curve of the Inconel 718 superalloy

Table 4 Characteristics of the equivalent circuit derived by the fitting of impedance

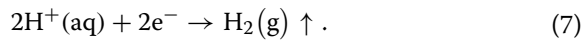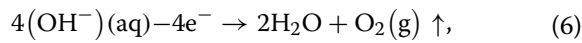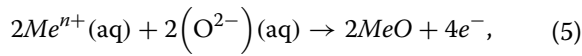| Equivalent component	Value	Error (%)
R (Ω/cm^2)	8.655	0.13
C (F/cm^2)	4.782×10^{-4}	2.6
R_1 (Ω/cm^2)	3.435	7.1
R_2 (Ω/cm^2)	1.571	1.3
L (H/cm^2)	0.0860	8.3
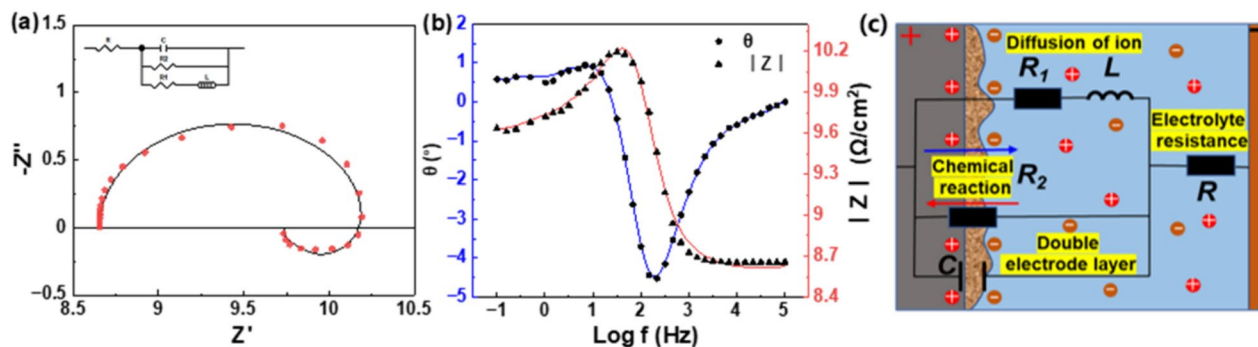
Figure 6 Electrochemical impedance spectroscopy and equivalent circuit: **a** Nyquist plot, **b** Bode plot, **c** Equivalent circuit

$$2Me^{n+}(\text{aq}) + 2\left(O^{2-}\right)(\text{aq}) \rightarrow 2MeO + 4e^-, \qquad (5)$$

$$4\left(OH^-\right)(\text{aq}) - 4e^- \rightarrow 2H_2O + O_2(g) \uparrow, \qquad (6)$$

$$2H^+(\text{aq}) + 2e^- \rightarrow H_2(g) \uparrow. \qquad (7)$$

4.2 Comparative Analysis of Electrolytic and PEP Modes

Material removal in PEP relies primarily on electrochemical reactions and is closely related to the characteristics of the VGE. To further understand the effects of the electrolytic and PEP modes on material removal and surface roughness, as well as verify the feasibility of the PUP-PEP processing method, comparative experiments were conducted in both modes. The material removal rates, current efficiencies, and surface qualities were compared and analysed.

Figure 7 presents a comparison of the processed signals and phenomena observed while maintaining a consistent average current density (0.43 A/cm^2) during the
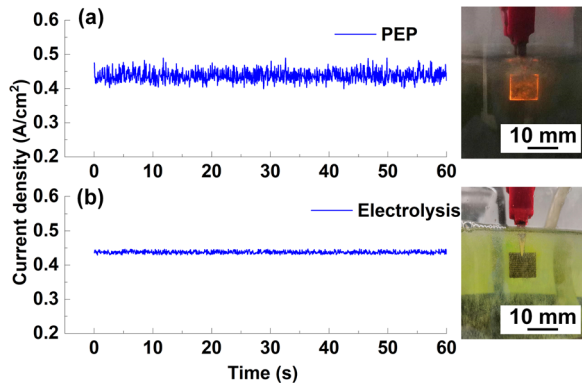
Figure 7 Current density and the phenomenon at PEP and electrolysis modes: **a** PEP, and **b** electrolysis
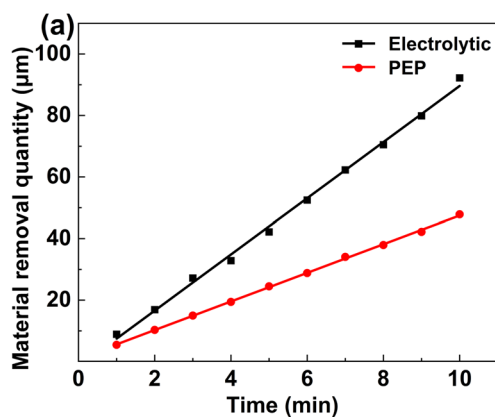
processing. When compared to the processing signal in the electrolytic mode, the signal in the PEP mode displayed significant fluctuates attributed to the oscillations of the VGE, as depicted in Figure 7(a). Furthermore, it is evident that in the PEP mode, the workpiece surface becomes coated with a layer of VGE accompanied by luminescence, and audible sounds of bubble collapse can be observed on-site. By contrast, the electrolytic mode is comparatively quieter but generates small bubbles on the workpiece surface, as shown in Figure 7(b). This constitutes one of the most noticeable distinctions between the PEP and electrolytic modes. A comparative analysis of the polishing effects of these two modes was conducted, revealing distinct differences in their polishing outcomes.

4.2.1 Material Removal Rate and Current Efficiency

Despite maintaining an identical current density in both the electrolytic and PEP modes, differences arose in the material removal and current efficiency. As depicted in Figure 8(a), the amount of material removed exhibited a direct proportionality to time in both modes, with the material removal rate in the electrolytic mode nearly double that observed in the PEP mode. Figure 8(b) illustrates the calculated current efficiency, revealing a range of 80% to 95% in the electrolytic mode, whereas, in the PEP mode, the current efficiency ranged from 50% to 65%.

In the electrolytic mode, the workpiece surface is in direct contact with the electrolyte. In addition to the formation of bubbles on the electrode surface, minimal Joule heating occurs. The vast majority of the electrical energy output from the power source is converted into chemical energy, which is used for electrochemical reactions. However, in the PEP mode, a portion of the energy must be converted into Joule heating to maintain the existence of the VGE. Consequently, the material removal rate and current efficiency in the electrolytic mode both surpassed those in the PEP mode.
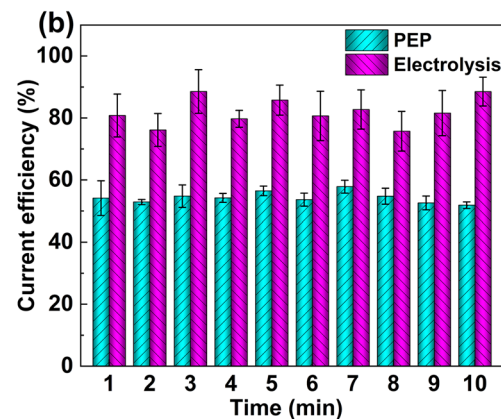

Figure 8 Material removal and current efficiency of the workpiece in two modes: **a** The amount of material removed, and **b** Current efficiency

Zhou *et al. Chinese Journal of Mechanical Engineering*   (2024) 37:105

Page 8 of 17

### 4.2.2 Surface Roughness and Surface Element Analysis

Although higher material removal rates and current efficiency can be achieved in electrolytic mode, a lower surface roughness cannot be obtained. As shown in Figure 9, with an increase in processing time, the surface roughness values of the workpieces in both the electrolytic and PEP modes show a decreasing trend. After 10 min of processing in the electrolytic mode, the surface roughness value of the workpiece decreases from the initial R_a 7.5 μm to R_a 4.6 μm. In comparison, after 10 min of processing in the PEP mode, the surface roughness of the workpiece can be reduced from the original R_a 6.9 μm to R_a 1.1 μm, which is lower than that achieved in the electrolytic mode.

The processing differences between the electrolytic and PEP modes are not only reflected in the surface roughness values but are also characterised using three-dimensional video microscopy and scanning electron microscopy to observe the surface morphology after both modes of processing. The results revealed that the surface of the workpiece after the PEP mode exhibited a smoother finish with no apparent residues on the cross-section, as shown in Figure 10(a) and (b). By contrast, the electrolysis mode left behind a layer of visible electrolysis products on the workpiece surface, as shown in Figure 10(c) and (d).

The energy spectrum analysis revealed that, except for a small number of oxygen elements, the major elements present on the workpiece surface after PEP were similar to those before polishing, as depicted in Figure 11(a). Interestingly, only the Fe and Cr compositions differed from those of the matrix. The iron content of the workpiece surface decreases significantly after polishing, whereas the chromium content increases significantly. This difference in composition can be attributed to the varying electrochemical dissolution rates of Fe and Cr, with the dissolution rate of Fe being higher than that of
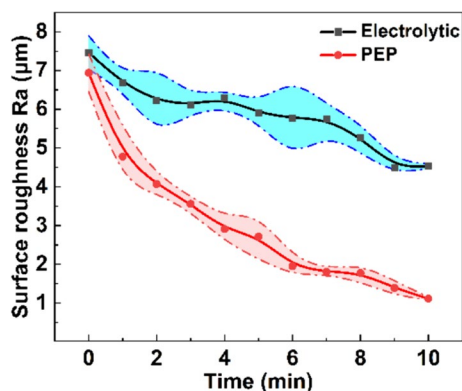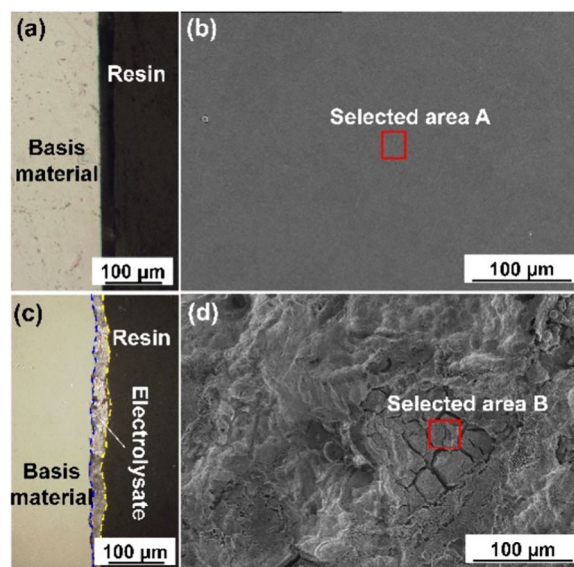
Figure 10 Cross-section and SEM of the surface at two modes: **a** and **b** after PEP, **c** and **d** after electrolysis

Cr. Similarly, the main element types in the electrolysis product were identical to those present before polishing; however, the contents of the other elements, except for chromium, were significantly different. This is because these other elements exist in ionic form in the electrolyte.

In addition, a substantial amount of oxygen is detected in the electrolysis products, as presented in Figure 11(b). In the electrolytic mode, the oxidation reaction on the workpiece surface generates a large number of metal oxides that tend to adhere to the workpiece surface, thereby impeding effective surface polishing. These findings underscore the superiority of the PEP mode in achieving an improved surface finish with minimal residue formation, thus providing valuable insights into the underlying material-removal mechanism of PUP-PEP.

Based on the comparative analysis presented above, it can be inferred that the VGE plays a crucial role in removing electrolytic products generated on the workpiece surface. This removal process is instrumental in understanding the material removal and surface smoothing mechanisms of PEP, which are the outcomes of the combined action of electrochemical and VGE [31].

To reflect the function of the VGE and plasma discharge more directly, the workpiece was first processed in the electrolytic mode for 60 s and then in the PEP mode for 10 s. As shown in Figure 12(a) and (b), after 60 s of electrolysis, a black layer of electrolytic product is formed compared to the original surface. Compared with the initial surface morphology, the processed workpiece surface has obvious black and bright areas, as shown in Figure 12(b). This is because black

Figure 9 Variation trend of surface roughness in PEP and electrolytic modes

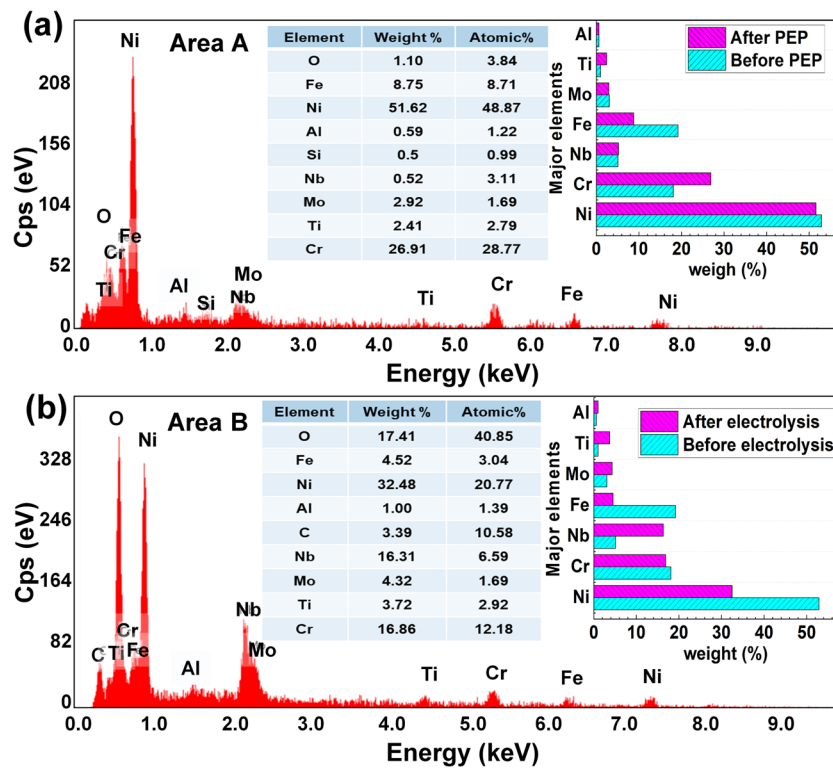**Figure 11** Surface energy spectrum analysis of workpiece under two modes: **a** PEP, and **b** Electrolysis
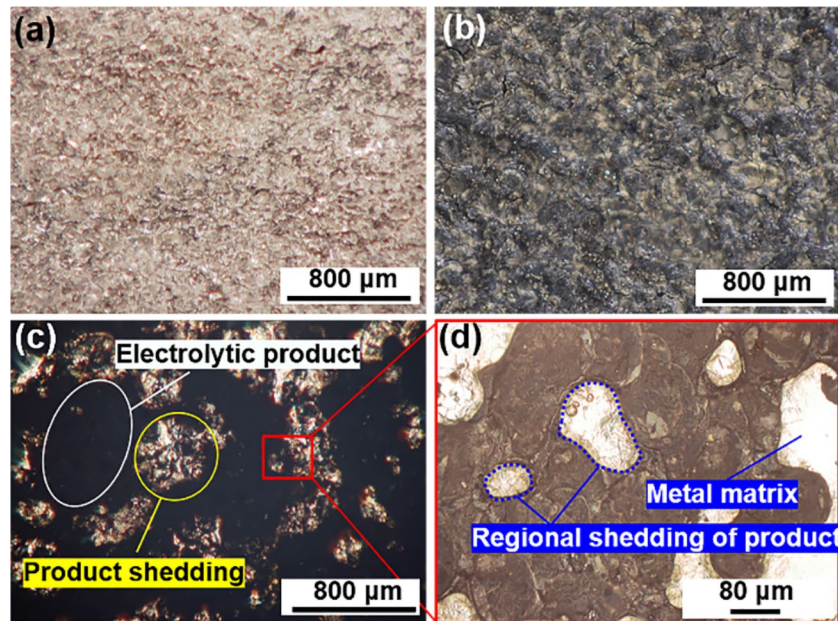

Figure 12 Localised detachment of electrolytic products: **a** Initial surface topography, **b** Surface morphology of the workpiece after 60 s of electrolysis, **c** Surface morphology after 60 s of electrochemical etching followed by 10 s of PEP, and **d** Enlarged view of a specific area

electrolytic products formed on the workpiece surface after 60 s of electrolysis and attached to the surface. After 10 s of PEP, under the fluctuations of VGE, the electrolytic products on the workpiece surface are selectively detached in certain areas, revealing a bright metallic substrate, as shown in Figure 12(c) and (d). At the same time, it cannot be ruled out that the impact of the plasma discharge may cause the detachment of electrolytic products from the workpiece surface. Hence, it is feasible to use the PUP-PEP method to reduce the surface roughness of workpieces with high surface roughness. The combined action of electrochemical and plasma discharges in PUP-PEP mode is a highly effective approach for achieving superior workpiece surface polishing.

4.3 Performance Evaluation of PUP-PEP

#### 4.3.1 Parameter Optimization of PUP-PEP

Based on a comprehensive analysis of the experimental results, it can be inferred that PUP-PEP has a notable effect on mitigating workpiece surface roughness.

Specifically, as evidenced in Table 5 and Figure 13(a), the experimental outcomes reveal that Group 3 exhibits the most favourable surface finish. Also, as shown in Figure 13(b), Group 3 exhibits a relatively high material removal rate. However, the current efficiency of Group 3 was not the highest; Group 6 had the highest. It is challenging to obtain a process parameter combination that comprehensively considers surface roughness, material removal rate, and current efficiency directly from the results of the orthogonal experiment. To obtain a comprehensive consideration of the optimal process parameter combination based on these three indicators, further analysis of the results from the orthogonal experiments is required.

To quantitatively assess the extent of influence exerted by each contributing factor on the test results, we employed the grey correlation analysis method to analyse and process the data obtained from the orthogonal tests. Furthermore, this method allows for parameter optimization across multiple indicators. Utilizing grey correlation analysis enabled the quantification of the influence

Table 5 Orthogonal test results

Exp. Nr	A Voltage	B Waveforms	C Periods	D Loading time	Roughness R_a (µm)	MRR (µm/min)	Current efficiency (%)
1	1	1	1	1	4.38	28.06	68.84
2	1	2	2	2	3.7	30.13	55.84
3	1	3	3	3	0.95	38.99	62.89
4	2	1	2	3	2.37	16.8	42.13
5	2	2	3	1	5.01	20.25	44.20
6	2	3	1	2	1.43	38.93	70.49
7	3	1	3	2	3.61	12.6	51.90
8	3	2	1	3	1.64	28.38	66.58
9	3	3	2	1	3.47	32.25	65.58
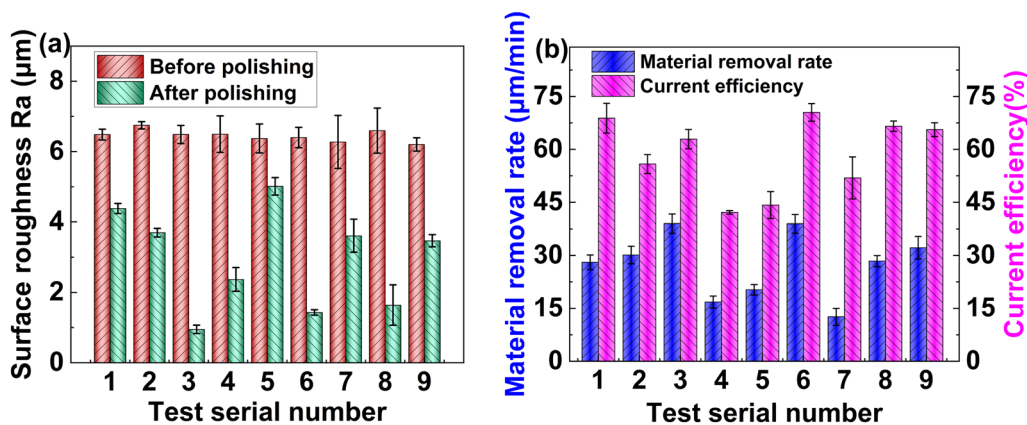
Figure 13 Orthogonal test results: **a** Surface roughness, and **b** Material removal rate and current efficiency

associated with each factor level. Subsequently, the results of the orthogonal tests underwent analysis and calculation using the grey correlation analysis method to ascertain the impact of each factor on polished surface roughness, material removal rate, and current efficiency. Due to the diverse nature of these factors and the non-standardised units they represent, it becomes imperative to standardise the results from orthogonal tests. Grey correlation analysis employs three primary data preprocessing approaches based on distinct desired outcomes: maximising the value, minimising the value, or achieving proximity to a specific numerical target. In our study, the primary objective was to minimise the surface roughness of the workpiece. Therefore, the roughness values in the orthogonal test table were standardised using Eq. (8). Conversely, the material removal rate and current efficiency serve as indicators of polishing efficiency for the workpiece surface, and the goal is to maximise these parameters. Thus, the material removal rate was standardised using Eq. (9). The results of the orthogonal test and the corresponding grey correlation analysis values are presented in Table 6.

$$x_i(k) = \frac{\max y_i(k) - y_i(k)}{\max y_i(k) - \min y_i(k)}, \tag{8}$$

$$x_i(k) = \frac{y_i(k) - \min y_i(k)}{\max y_i(k) - \min y_i(k)}, \tag{9}$$

where $x_i(k)$ is the corresponding normalised value under index k, and $y_i(k)$ is the test result of group i under index k. The corresponding correlation coefficient $\varepsilon_i(k)$ can be obtained by processing the normalised data according to Eq. (10):

$$\varepsilon_i(k) = \frac{\Delta_{min} + \rho \cdot \Delta_{max}}{\Delta_i(k) + \rho \cdot \Delta_{max}}, \tag{10}$$

where ρ is the discrimination coefficient (the value is generally 0.5), and $\Delta_i(k)$ is the absolute difference between the normalised value $x_i(k)$ and the reference value 1, corresponding to the group of i under the indicator of k ($\Delta_i(k) = |x_i(k) - 1|$). Δ_{min} and Δ_{max} are the minimum and maximum values of $\Delta_i(k)$, respectively.

The grey correlation coefficient $\varepsilon_i(k)$ represents the degree of correlation between the reference sequence $X_0(k)$ and the comparison sequence $X_i(k)$. The reference sequence can be regarded as a certain result, whereas the comparison sequence can be understood as the sequence that causes the result. The correlation coefficient can be understood as the degree to which the causality holds. In this study, the surface roughness, material removal rate, and current efficiency have the same weight, so the correlation degree γ_i between the actual test scheme and the ideal test scheme is:

$$\gamma_i = \frac{1}{n} \sum_{k=1}^{n} \varepsilon_i(k). \tag{11}$$

Table 6 reveals that the degree of correlation corresponding to Group 6 was the closest to 1. This indicates that, within the specific combination of process parameters tested in the third group of nine experiments, considering the three indices of surface roughness, material removal rate, and current efficiency, the polishing effect is optimal. It is important to note that the parameter combinations considered in this study are limited to those included in the orthogonal experimental matrix. However, the process parameter combination that aligns most closely with ideal experimental results may not necessarily be present within an orthogonal experimental matrix.

In elucidating the impact of process parameters on surface roughness, material removal rate, and current efficiency during polishing, the average correlation coefficient was calculated for each level of every factor

Table 6 Orthogonal test results and correlation degree according to Eqs. (8)–(11)

Exp. Nr	Parameter	$x_i (R_a)$	x_i (MRR)	x_i (%)	$\varepsilon_i (R_a)$	ε_i (MRR)	ε_i (%)	γ_i
1	$A_1B_1C_1D_1$	0.155	0.586	0.940	0.372	0.547	0.893	0.6039
2	$A_1B_2C_2D_2$	0.323	0.664	0.482	0.425	0.598	0.491	0.5048
3	$A_1B_3C_3D_3$	1.000	1.000	0.732	1.000	1.000	0.651	0.8838
4	$A_2B_1C_2D_3$	0.650	0.159	0.000	0.588	0.373	0.333	0.4315
5	$A_2B_2C_3D_1$	0.000	0.290	0.074	0.333	0.413	0.351	0.3657
6	$A_2B_3C_1D_2$	0.882	0.998	1.000	0.809	0.995	1.000	0.9347
7	$A_3B_1C_3D_2$	0.345	0.000	0.345	0.433	0.333	0.433	0.3997
8	$A_3B_2C_1D_3$	0.830	0.598	0.863	0.746	0.554	0.785	0.6950
9	$A_3B_3C_2D_1$	0.379	0.743	0.827	0.446	0.743	0.743	0.6166

Zhou *et al. Chinese Journal of Mechanical Engineering* (2024) 37:105

Page 12 of 17
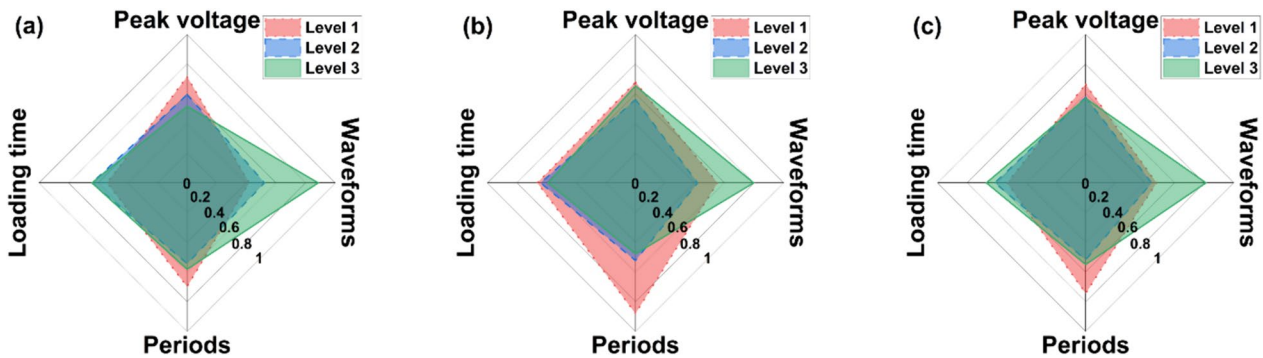
Figure 14 Average values of correlation coefficients corresponding to each factor level: **a** Correlation coefficients for surface roughness, **b** Correlation coefficients for material removal rate, **c** Correlation coefficients for current efficiency

listed in the orthogonal test table. This average coefficient serves as an indicator of how closely each process parameter level aligns with the optimal testing parameter, allowing for a quantitative assessment of their respective influences. Furthermore, the range of mean correlation coefficient values corresponding to different levels of the same factor represents the extent of influence exerted by that factor on achieving the desired test results. Figure 14(a) illustrates the range of correlation coefficients for the three levels associated with each factor influencing machined surface roughness. Notably, the waveform exhibited the largest correlation coefficient range, followed by peak voltage, period, and loading time, as depicted in Figure 15. This finding suggests that the waveform has the most significant influence on attaining the desired surface roughness, with peak voltage, period, and loading time following in decreasing order of importance. Additionally, the correlation coefficients linked to Level 1 peak voltage, Level 3 waveform, Level 1 period, and Level 3 loading time are the highest among their respective levels, signifying their utmost influence. Therefore, it is advisable to employ parameter combination $A_1B_3C_1D_3$ to achieve minimal surface roughness in the machined workpiece.

Similarly, Figure 14(b) and (c) depict the degree of influence on the material removal rate and current efficiency, respectively. The impact on the material removal rate ranked in the following order, from greatest to least: period, waveform, peak voltage, and loading time. By contrast, the degree of influence on ionization efficiency followed this order, from greatest to least: waveform > period > loading time > peak voltage. The recommended parameter combination for achieving a high material removal rate is $A_1B_3C_1D_1$, whereas the parameter combination recommended for achieving high current efficiency is $A_1B_3C_1D_3$.

The analysis revealed that the combination of process parameters resulting in reduced surface roughness and high current efficiency was $A_1B_3C_1D_3$, whereas the combination of process parameters leading to a high material removal rate was $A_1B_3C_1D_1$. It is important to note that the above-mentioned process parameter combinations were determined with a focus on optimising a single index each. For a more comprehensive perspective, the average degree of correlation for each level of process parameters was calculated by averaging the correlation values corresponding to the same factor and level. This is illustrated in Table 7, where the average correlation value for A_1 (250 V), for instance, is calculated by averaging the correlation degrees from groups 1–3 of the tests, as detailed in Table 6. Table 7 displays the resulting average degree of correlation for each level of PUP-PEP parameters (peak voltages, waveforms, periods, loading time).

The process parameters combination for PUP-PEP was determined by comprehensively considering the values of surface roughness, material removal rate, and current efficiency. As shown in Figure 16(a), the experimental results were closest to the ideal when the peak voltage was 250 V (level 1), the voltage waveform was triangular (level 3), the period was 0.5 s (level 1), and the machining
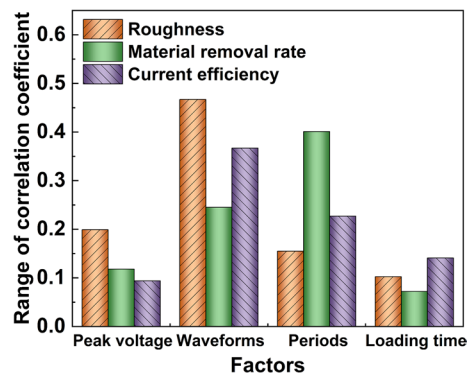
Figure 15 Range of correlation coefficients corresponding to each factor level

Table 7 Average correlation degree of each level of process parameters

Serial number	Level 1	Level 2	Level 3	Range	Factors
A	0.664	0.577	0.570	0.094	Peak voltage (V)
B	0.478	0.521	0.812	0.334	Waveforms
C	0.745	0.518	0.550	0.227	Periods (s)
D	0.529	0.613	0.644	0.115	Loading time (min)

time was 3 min (level 3). Therefore, these values were chosen as the experimental parameters for PUP-PEP. Additionally, from Figure 16(b), it can be observed that the order of the impact magnitude of the four factors on the experimental results is as follows: waveform, period, loading time, and peak voltage.
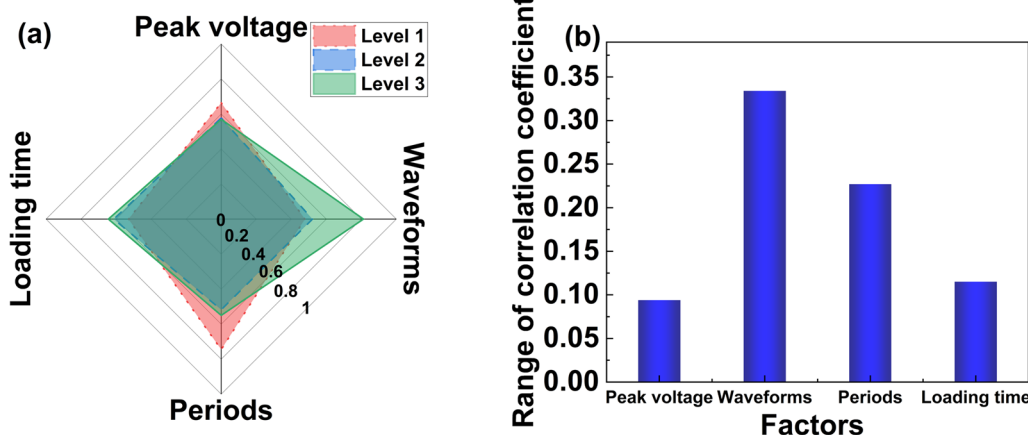
4.3.2 Verification of Optimal Process Parameters

Experimental verification was conducted using the optimized process parameters. The surface topographies of the workpiece before and after polishing are illustrated in Figure 17(a) and (b), respectively. The workpiece surface became noticeably smoother and flatter following the polishing process. The initial surface height difference of the workpiece, which stood at 69 μm, was substantially reduced to 14 μm, as depicted in Figure 17(c) and (d). Moreover, the section profile of the workpiece surface appeared remarkably uniform. Figure 17(e) highlights that within a 3-min timeframe, the surface roughness was reduced from its initial R_a 7.39 μm to R_a 0.78 μm. By contrast, traditional PEP required 10 min to reduce the surface roughness of the workpiece from R_a 6.9 μm to R_a 1.1 μm, as shown

in Figure 9. In comparison to traditional PEP, PUP-PEP can enhance polishing efficiency by a minimum of 233%.

Similarly, the material removal rate of PUP-PEP is 37.12 μm/min, which is 7.77 times that of the traditional PEP, as shown in Figure 18. Furthermore, under the optimised process parameters, the polishing current efficiency of PUP-PEP was significantly higher (72.24%) than that of the traditional PEP. However, there are limitations to optimising the process parameter combination using this approach, namely, the fixed range and levels of the process parameters. Despite this, it significantly improved the polishing efficiency and surface quality, providing a valuable reference for the extended application of PEP.

The impact of waveforms on the surface roughness and material removal rate is substantial, with the triangular waveform voltage demonstrating the most favourable trade-off between the quality and efficiency of the machined surface. This is because the duration of the electrolysis (**E**) mode for the triangular waveform voltage was longer than that of the PEP (**P**) mode in one period, as shown in Figure 19(a). However, the voltages of the square and sinusoidal waveforms essentially experienced the same duration of electrolysis and PEP modes in one period, as shown in Figure 19(b) and (c). Material removal during PUP-PEP relies primarily on electrochemical reactions. The triangular waveform voltage affords a longer electrochemical reaction time, leading to improved polishing surface quality and efficiency compared with square or sinusoidal waveforms. Of course, this does not mean that the longer the proportion of electrolytic time, the better, because the PEP mode also needs a certain amount of time to

Figure 16 The correlation of process parameters to experimental results: **a** Average degree of association for each factor level and range, **b** Range of correlation coefficient
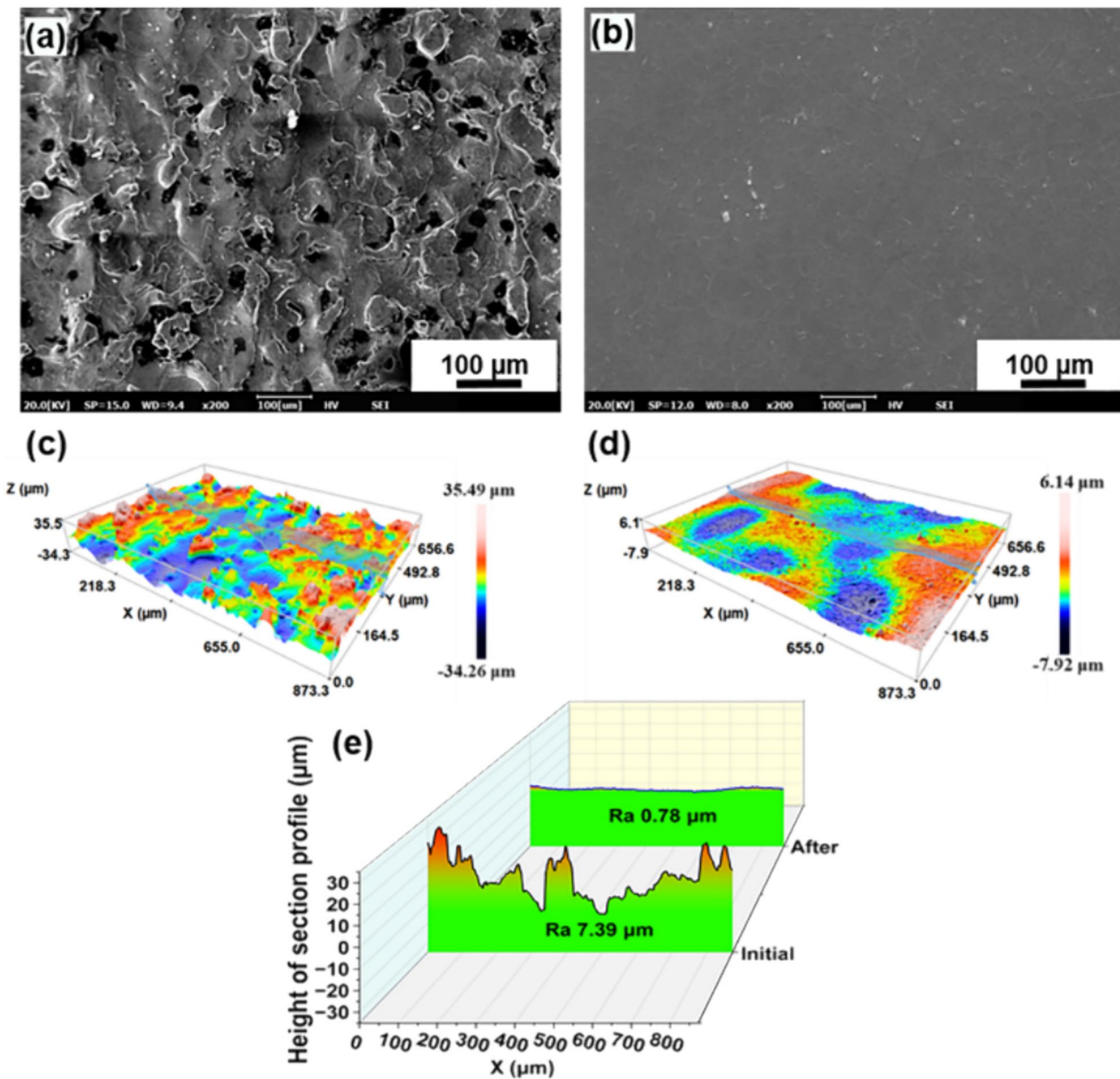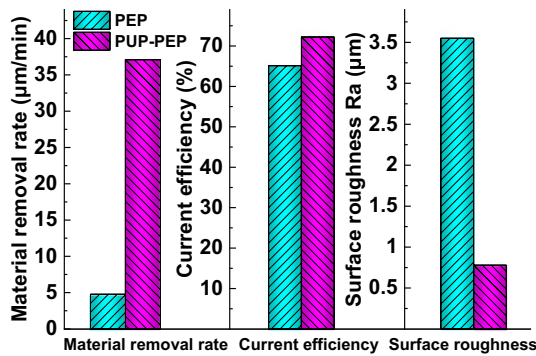
Figure 17 Polishing effect of workpiece surface under optimal process parameters: **a** SEM image of the initial surface, **b** SEM image of the surface after polishing, **c** 3D topography of the initial surface, **d** 3D topography of workpiece surface after polishing, and **e** Section profile of workpiece surface before and after polishing

completely remove the electrolytic products generated in the electrolytic mode.

The findings of this study unequivocally demonstrate that PUP-PEP serves as an effective means to enhance the surface quality of a workpiece. However, it is important to note that the achieved surface roughness through this processing method does not necessarily represent the final state, as there exists potential for further reduction in the workpiece's surface roughness value. As shown in Figure 20(a) and (b), by employing the PUP-PEP method, the workpiece's surface roughness can be swiftly reduced to approximately R_a 1 μm, and this value can be further diminished through the application of traditional PEP techniques. Realising the full potential of PUP-PEP hinges on the precise control of the output voltage waveform using a programmable DC power supply. Consequently, following the completion of PUP-PEP, the control power supply can be used to sustain the DC voltage output within the range of 250 V–400 V, facilitating the continuation of PEP on

Figure 18 Comparison of the polishing effects between PUP-PEP under optimized parameters and traditional PEP

the workpiece, as shown in Figure 20(d). This sequential process is expected to achieve the final finishing of the workpiece's surface. For instance, transforming the voltage to 250 V and continuing the polishing process for 3 min can reduce the workpiece's surface roughness from R_a 0.78 μm to R_a 0.27 μm, as shown in Figure 20(b) and (c).

5 Conclusions

In this study, a novel surface machining technology, PUP-PEP, was introduced. It can efficiently achieve a high surface quality for workpieces with high surface roughness. The key conclusions are as follows:

(1) PUP-PEP combines the electrolytic and PEP modes by coordinating the output voltage. As a result, PUP-PEP seamlessly integrates the benefits of the electrolytic mode, which offers high material removal efficiency, with the PEP mode, providing a high surface quality. During the electrolytic mode, the electrolyte and workpiece undergo an electrochemical reaction, which removes materials with high efficiency. In the PEP mode, the fluctuates of VGE, and the plasma discharge result in the removal of electrolytic products, thereby reducing workpiece surface roughness.

(2) The voltage waveform plays a crucial role in determining surface roughness, material removal rate, and current efficiency. Modifying the voltage waveform increases current density during the PUP-PEP process, with the triangular waveform proving to be the most effective. This is due to the workpiece spending more time in the electrolytic mode under the triangular waveform voltage, resulting in a higher current density and exceptional polishing performance.

(3) Under the optimal PUP-PEP process parameters, the surface roughness of the workpiece can be reduced from R_a 7.39 μm within the first 3 min dropped to R_a 0.78 μm. Continuing to polish the workpiece under the DC voltage stabilization conditions for 3 min can reduce the surface roughness of the workpiece to R_a 0.27 μm. This study establishes PUP-PEP as an effective method for machining workpieces with initially high surface roughness.

The proposed PUP-PEP has demonstrated exceptional performance in terms of efficiency and surface quality. It has a great potential to replace conventional rough-finish machining processes, e.g., cutting-grinding-finishing, which is commonly used in post-processing for near-net fabrication processes.
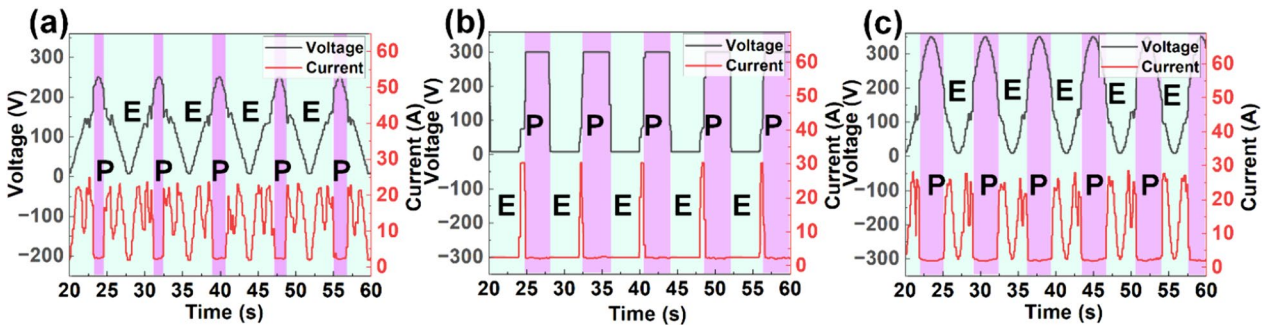
Figure 19 Polishing current signals under different voltage waveforms: **a** Triangle wave, **b** Square wave, **c** Sine wave (**E** and **P** stand for electrolysis and PEP, respectively)
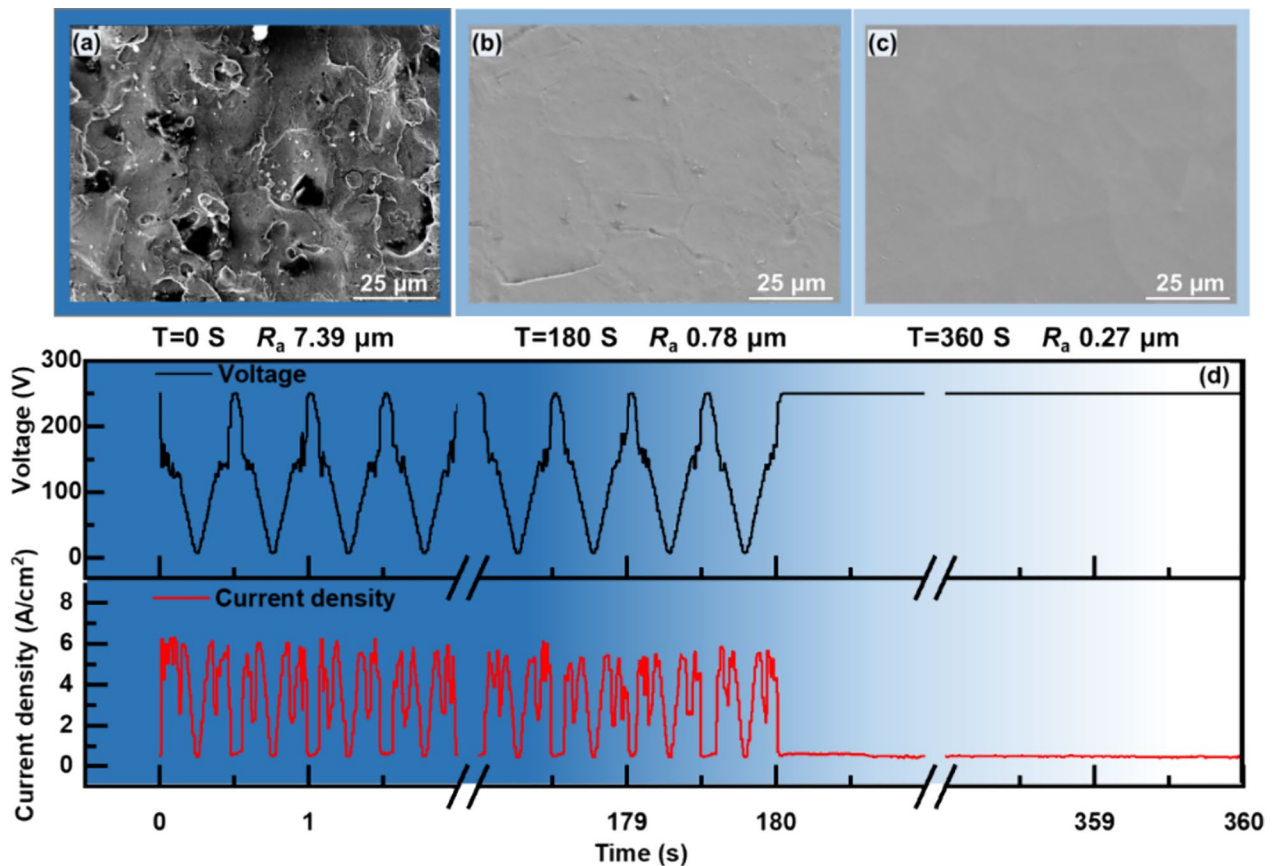
Figure 20 SEM images of workpiece surface at different processing stages: **a** Initial surface morphology, **b** PUP-PEP processing for 3 min, **c** Continued PEP processing for 3 min, **d** Voltage and current signals

Author Contributions
CZ, NQ, and HS were in charge of the whole trial; CZ wrote the manuscript; JH, WD, and JX assisted with sampling and laboratory analyses. All authors read and approved the final manuscript.

Data availability
The datasets supporting the conclusions of this article are included within the article.

Declarations

Competing Interests
The authors declare no competing financial interests.

References
[1] D D Gu, X Y Shi, R Poprawe, et al. Material-structure-performance integrated laser-metal additive manufacturing. *Science*, 2021, 372: 6545.
[2] M A Sadiq, N M Hoang, N Valencia, et al. Experimental study of micromilling selective laser melted Inconel 718 superalloy. *Procedia Manufacturing*, 2018: 26.
[3] M Machno, E Franczyk, R Bogucki, et al. A comparative study on the structure and quality of slm and cast AISI 316L samples subjected to WEDM processing. *Materials*, 2022, 15: 701.
[4] B C Zhang, X H Lee, J Bai, et al. Study of selective laser melting (SLM) Inconel 718 part surface improvement by electrochemical polishing. *Materials and Design*, 2017, 116: 531–537.
[5] P Sharma, D Chakradhar, S Narendranath. Evaluation of WEDM performance characteristics of Inconel 706 for turbine disk application. *Materials and Design*, 2015, 88: 558–566.
[6] J Boban, A Ahmed, E K Jithinraj, et al. Polishing of additive manufactured metallic components: retrospect on existing methods and future prospects. *The International Journal of Advanced Manufacturing Technology*, 2022, 121(1–2): 83–125.
[7] C Q Zhou, H H Su, N Qian, et al. Characteristics and function of vapour gaseous envelope fluctuate in plasma electrolytic polishing. *The*

International Journal of Advanced Manufacturing Technology, 2022, 119 (11–12): 7815–7825.

[8] E V Parfenov, A Yerokhin, R R Nevyantseva, et al. Towards smart electrolytic plasma technologies: An overview of methodological approaches to process modelling. *Surface & Coatings Technology*, 2015, 269: 2–22.

[9] Y Huang, C Y Wang, F Ding, et al. Principle, process, and application of metal plasma electrolytic polishing: a review. *The International Journal of Advanced Manufacturing Technology*, 2021, 114(7–8): 1893–1912.

[10] S Y Shadrin, A V Zhirov, P N Belkin. Thermal features of plasma electrolytic heating of titanium. *International Journal of Heat and Mass Transfer*, 2017, 107: 1104–1109.

[11] A Yerokhin, V R Mukaeva, E V Parfenov, et al. Charge transfer mechanisms underlying contact glow discharge electrolysis, *Electrochimica Acta*, 2019, 312: 441–456.

[12] I Danilov, M Hackert-Oschätzchen, M Zinecker, et al. Process understanding of plasma electrolytic polishing through multiphysics simulation and inline metrology. *Micromachines*, 2019, 10(3): 214.

[13] H P Schulze, H Zeidler, O Kröning, et al. Process analysis of plasma-electrolytic polishing (PeP) of forming tools. *International Journal of Material Forming*, 2022, 15(1): 6.

[14] E V Parfenov, R G Farrakhov, V R Mukaeva, et al. Electric field effect on surface layer removal during electrolytic plasma polishing. *Surface & Coatings Technology*, 2016, 307: 1329–1340.

[15] A Spica, J Roche, L Arurault, et al. Evolution of model roughness on quasi-pure aluminum during plasma electrolytic polishing. *Surface & Coatings Technology*, 2021, 428: 127839.

[16] T R Ablyaza, K R Muratova, M M Radkevichb, et al. Electrolytic plasma surface polishing of complex components produced by selective laser melting. *Russian Engineering Research*. 2018, 38(6): 491–492.

[17] S Quitzke, O Kröning, D Safranchik, et al. Design and setup of a jet-based technology for localized small scale Plasma electrolytic polishing. *Journal of Manufacturing Processes*, 2022, 75: 1123–1133.

[18] Y L Wu, L Wang, J Y Zhao, et al. Spray electrolyte plasma polishing of GH3536 superalloy manufactured by selective laser melting. *The International Journal of Advanced Manufacturing Technology*, 2022, 123 (7–8): 2669–2678.

[19] J Wang, L C Suo, L L Guan, et al. Optimization of processing parameters for electrolysis and plasma polishing. *Applied Mechanics and Materials*, 2012, 217–219: 1368–1371.

[20] R R Nevyantseva, S A Gorbatkov, E V Parfenov, et al. The influence of vapor-gaseous envelope behavior on plasma electrolytic coating removal. *Surface & Coatings Technology*, 2001, 148 (1): 30–37.

[21] Y C Ge, Z W Zhu, D Y Wang. Electrochemical dissolution behavior of the nickel-based cast superalloy K423A in $NaNO_3$ solution. *Electrochimica Acta*, 2017, 253: 379–389.

[22] P N Belkin, S A Kusmanov, E V Parfenov. Mechanism and technological opportunity of plasma electrolytic polishing of metals and alloys surfaces. *Applied Surface Science Advances*, 2020, 1: 100016.

[23] H Zeidler, F Boettger-Hiller, J Edelmann, et al. Surface finish machining of medical parts using plasma electrolytic polishing. *Procedia CIRP*, 2016, 49: 83–87.

[24] M M Basha, S M Basha, V K Jain, et al. State of the art on chemical and electrochemical based finishing processes for additive manufactured features. *Additive Manufacturing*, 2022, 58: 103028.

[25] L Q Yang, N Laugel, J Housden, et al. Plasma additive layer manufacture smoothing (PALMS) technology – An industrial prototype machine development and a comparative study on both additive manufactured and conventional machined AISI 316 stainless steel. *Additive Manufacturing*, 2020, 34: 101204.

[26] B Seo, H Park, H G Kim, et al. Corrosion behavior of additive manufactured CoCr parts polished with plasma electrolytic polishing. *Surface & Coatings Technology*, 2021, 406: 126640.

[27] S V Zakharov, M T Korotkikh. Electrolytic plasma processing of complex products from aluminum alloy D16. *Journal of Almaz – Antey Air and Defence Corporation*, 2017, 3: 83–87.(in Russian)

[28] R I Valiev, A A Khafizov, Y I Shakirov, et al. Polishing and deburring of machine parts in plasma of glow discharge between solid and liquid electrodes. *IOP Conference Series: Materials Science and Engineering*, 2015, 86: 12026.

[29] M K Smyslova, D R Tamindarov, N V Plotnikov, et al. Surface electrolytic-plasma polishing of Ti-6Al-4V alloy with ultrafine-grained structure produced by severe plastic deformation. *IOP Conference Series: Materials Science and Engineering*, 2019, 461: 12079.

[30] C Q Zhou, N Qian, H H Su, et al. Effect of energy distribution on the machining efficiency and surface morphology of Inconel 718 nickel-based superalloy using plasma electrolytic polishing. *Surface & Coatings Technology*, 2022, 441: 128506.

[31] F Su, H Yang, W Wu, et al. An electrolyte life indicator for plasma electrolytic polishing optimization. *Applied Sciences*, 2022, 12: 8594.

[32] P Gupta, G Tenhundfeld, E O Daigle, et al. Electrolytic plasma technology: Science and engineering—An overview. *Surface & Coatings Technology*, 2007, 201: 8746–8760.

[33] J Wang, L C Suo, Y L Fu. Study on material removal rate of electrolysis and plasma polishing. *IEEE International Conference on Information and Automation (ICIA)*, Shenyang, China, June, 2012: 917–922.

[34] Y Cao, Y J Zhu, W F Ding, et al. Vibration coupling effects and machining behavior of ultrasonic vibration plate device for creep-feed grinding of Inconel 718 nickel-based superalloy. *Chinese Journal of Aeronautics*, 2022, 35(2): 332–345.

[35] A Thakur, S Gangopadhyay. State-of-the-art in surface integrity in machining of nickel-based super alloys. *International Journal of Machine Tools and Manufacture*, 2016, 100: 25–54.

[36] Z W Rao, G D Xiao, B Zhao, et al. Effect of wear behaviour of single mono- and poly-crystalline CBN grains on the grinding performance of Inconel 718. *Ceramics International*, 2021, 47: 17049–1705.

Chuanqiang Zhou   born in 1991, is currently a Ph.D. candidate at *College of Mechanical and Electrical Engineering, Nanjing University of Aeronautics and Astronautics, China*. His main research interests include plasma electrolytic polishing.

Ning Qian   is currently an associate professor at *Jiangsu Key Laboratory of Precision and Micro-Manufacturing Technology, Nanjing University of Aeronautics and Astronautics, China*. He received his bachelor's and Ph.D. degrees from *Nanjing University of Aeronautics and Astronautics, China*, in 2016 and 2021. His research interests include high performance machining of difficult-to-cut alloys.

Honghua Su   is currently a professor at *Jiangsu Key Laboratory of Precision and Micro-Manufacturing Technology, Nanjing University of Aeronautics and Astronautics, China*. His research interests include high-efficiency precision machining of difficult materials.

Jingyuan He   is a Ph.D. candidate at *Nanjing University of Aeronautics and Astronautics*, majoring in hard and brittle materials processing and ultrasound-assisted machining technology.

Wenfeng Ding   is currently a professor at *Jiangsu Key Laboratory of Precision and Micro-Manufacturing Technology, Nanjing University of Aeronautics and Astronautics, China*. His research interests include high performance machining of difficult-to-cut alloys.

Jiuhua Xu   is currently a professor at *Jiangsu Key Laboratory of Precision and Micro-Manufacturing Technology, Nanjing University of Aeronautics and Astronautics, China*. His research interests include high performance machining of difficult-to-cut alloys.